ISSN 1054-660X, Laser Physics, 2009, Vol. 19, No. 5, pp. 1169–1178.

Comparison of Nano- and Femtosecond Laser Ablation of Aluminum[1]

V. I. Mazhukin, A. V. Mazhukin, and M. G. Lobok

Institute of Mathematical Modeling of Russian Academy of Sciences, Miusskaya sq. 4a, Moscow, 125047 Russia

e-mail: immras@orc.ru

Received November 14, 2008

Abstract—For mathematical description of pulsed laser heating, melting and evaporation of aluminum target in ambient atmosphere was used one dimensional, multi front hydrodynamic Stephan problem, written for both phases (liquid and solid). On the boundary of solid and gaseous forms Stephan problem is combined with radiation gas dynamic equations, with thermo conductivity, and describes processes in evaporated material and surrounding gas. For numerical solution finite difference dynamic adaptation method, which gives opportunity of explicit tracking of inter phase boundaries and shockwaves. As a result, in the process of the solution the problem had 6 computation regions and 7 boundaries, 6 of them were moving, including 2 shockwaves and free boundary in atmosphere. We used this model to calculate pulsed laser interaction with aluminum target with following parameters: $A = 0.8$, $\tau = 10^{-8}$–10^{-15} s and $G_0 = 10^9$–10^{16} W/cm^2. Modeling revealed that in case of long ~1 ns pulses greater part of the energy is spend on melting and heating of the liquid. Molten pool depth is about 1.2 μm. In case of femtosecond pulses greater part of the energy is spent on heating of the solid and for the formation of shockwave in solid. The depth of the molten pool does not exceeds 0.03 μm. Although evaporated layers were almost the same thickness. For nanosecond laser pulses with fluence J less than 30 J/cm^2, there is no plasma formation in the evaporated material. For the same fluence for femtosecond laser pulse plasma is formed after the pulse and has thermal nature.

PACS numbers: 79.20.Ds, 52.38.Ph

DOI: 10.1134/S1054660X0905048X

INTRODUCTION

The major parameters of interaction in pulsed laser applications along with a wavelength λ are intensity G and a pulse length τ. Two processes: the ablation of a material and the plasma formation are dominating in laser handling [1]. In case of plasma formation dynamics of these processes appears interconnected [2].

Influence a pico and femtosecond laser pulses of great intensity $G = 10^{15}$–10^{18} W/cm^2 on solid targets, is one of the methods to create plasma with unique properties. Thin, $l \sim 0.1$ μm, the plasma layer formed on a surface of the target by the overstrong light field, has high electronic temperature $T \sim 100$ eV density of charged particles $N_e \sim 10^{22}$–10^{23} cm^{-3} and high gradients of electrons and ions. Such plasma emites powerful X-rays [3, 4], which is one of the reasons of heightened interest to it.

Some of widely used technologies are based on pulsed laser ablation of metals, such as drilling, cutting, micro- and nanostructuring, film sputtering [5]. In laser applications based on laser ablation, plasma and its evolution, play a negative role in most cases, but presents independent interest.

Effects of long and short pulses are qualitatively different due to different mechanisms of laser energy conversion and removal of matter from the irradiated area. In the millisecond length range, the main mechanisms of matter removal are related to hydrodynamic phenomena: thermocapillarity, backpressure, etc. [6]. Instability of a number of processes is a distinctive feature of hydrodynamic mechanisms [7].

In microsecond and submillisecond ranges along with hydrodynamic phenomenona the role of phase transitions (melting and evaporation) becomes important. The simulations [8] showed that dominance of one process over another in many respects depends on a temporal pulse shape. If the energy impact is accelerated during the pulse (rising triangle) or the stationarity of processes is archived (top hat pulse shape), the mechanism of evaporation is dominating and the relation for a molten pool Δ_1 and the evaporated material Δ_{ev} is fulfilled $\Delta_1/\Delta_{ev} \ll 1$. For pulses with falling temporal pulse profile and other profiles which do not have constant component (gaussian profile) melting process becomes dominant and $\Delta_1/\Delta_{ev} \gg 1$.

In the nanosecond range the role of evaporation and laser plasma [9, 10] gaining more importance. In some regimes volume boiling competes of the surface evaporation mechanism [11].

Laser ablation in pico- and femtosecond ranges is least investigated. At the same time, the number of publications in this field is steadily growing which testifies to a heightened interest in impact of ultrashort laser

[1] The article is published in the original.

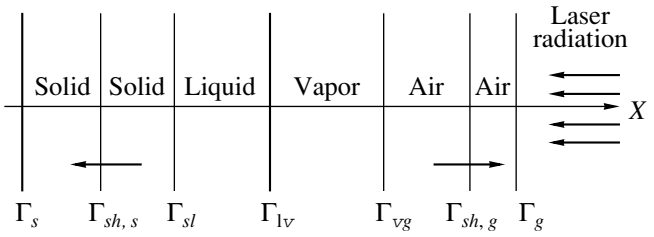

Fig. 1. Phase states spatial distribution.

pulses of great intensity on condensed media [12, 13]. Most of these works are concerned with experimental observations [14–16], A far smaller number of works attempt to provide a theoretical explanation of fundamental phenomena accompanying ultrashort exposure [17–19].

The main features of metals ultrashort exposure are related to high velocity and a volumetric nature of laser pulse energy release. High velocity of the condensed medium heating is related to fast phase transformations of matter characterized by powerful interphase fluxes of mass and energy. Energy being removed by a flux of matter combined with the volumetric laser radiation energy release mechanism contribute to heating of the interphase boundaries to temperatures that are significantly higher than the equilibrium melting temperatures T_{m0} and evaporation temperatures T_b. The same reasons account for formation of temperature maximum areas near the irradiated surfaces in solid and liquid phases.

At first, the superheated metastable states were discovered and investigated in nanosecond pulse range [20]. In one of the first publications [21], the overheating of a solid phase on 40–110 K higher than T_{m0} was observed for a 26 ns laser pulse influence on. In theoretical works [22, 23] by means of mathematical simulation, the dynamics of superheated metastable states in the superconducting ceramics irradiated by nanosecond laser pulse has been discussed. The peak overheating of a solid phase above T_m was 150 K.

As laser technology developed, reports [24] and articles [25–27] appeared concerned with observing overheated metastable states in pico- and femtosecond exposure ranges.

Summing up the deliverables of experimental research [15] on drilling of metals using ultrashort pulses, we would like to note the following peculiarities and advantages thereof:

—transition from nano- to femtosecond length reduces the share of liquid fraction and improves the quality of the hole,

—at energy density of laser pulse $J \le 5$ J/cm^2 a pico- and femtosecond duration there is no plasma formations,

—effects of a thermal conduction are not essential at laser pulse time scale,

—the average thickness of the evaporated material at $J \le 1$ J/cm^2 does not exceed 100 nm.

It is necessary to note a special role played by the dynamics of complex interrelated processes in the condensed and gas media in forming the macroprocess on the whole. For instance, dynamics of plasma processes is closely connected to heating, cooling and phase transformation processes in the irradiated target. And thermal conductivity and ablation determine the plasma cooling dynamics following exposure to a laser pulse. At the same time, research of the processes dynamics, especially where ultrashort pulses are applied, is related to constraints that are hard to overcome. As a rule, experimental observations represent an aftereffect, which is not sufficient to understand why the system acquires a certain state as a result of the exposure. Under such conditions, the role and weighting of mathematical modeling increase drastically.

This work is devoted to mathematical modeling of phase transitions dynamics, superheated metastable states and the comparative analysis of the main features of a laser ablation in pico- and femtosecond range.

PROBLEM STATEMENT

The laser beam propagates from right to left and, as it reaches the surface of the metal target, is partly absorbed and partly reflected, Fig. 1. The same Fig. 1 provides spatial distribution of phases, interphase boundaries Γ_{sl}. Γ_{lv} and shockwaves $\Gamma_{sh,s}$, $\Gamma_{sh,g}$.

The problem was stated under the following assumptions and constraints:

—laser energy is released in the direction of the lattice of the target instantaneously;

—phase transformations are thermal in nature;

—volumetric melting and evaporation mechanisms are not looked at. It is assumed that the melting front appears on the irradiated surface when the surface temperature rises up to T_{m0};

—overheated metastable states behave steady during the examination.

Mathematical description and modeling of laser ablation of solid aluminum target in counter pressure environment is implemented within the one dimensional multiphase hydrodynamic Stefan's problem formulated for both liquid and solid phase. Stefan's problem is related to a system of equations of radiation gas dynamics with thermal conductivity describing the processes in the evaporated matter and the gaseous medium (air):

$$\left[\begin{array}{c} \frac{\partial \rho}{\partial t} + \frac{\partial(\rho u)}{\partial x} = 0, \\ \frac{\partial(\rho u)}{\partial t} + \frac{\partial(\rho u^2)}{\partial x} + \frac{\partial P}{\partial x} = 0, \\ \frac{\partial(\rho\varepsilon)}{\partial t} + \frac{\partial(\rho u\varepsilon)}{\partial x} = -\left(P\frac{\partial u}{\partial x} + \frac{\partial W_T}{\partial x} + \frac{\partial W_I}{\partial x} + \frac{\partial G}{\partial x}\right), \\ \frac{\partial I_\nu}{\partial x} + \kappa(h\nu, \rho, T)I_\nu = \kappa(h\nu, \rho, T)I_{\nu,\mathrm{eq}}, \\ W_\nu = \int_0^\infty \int_{-1}^{1} \mu I_\nu d\nu d\mu, \quad W_T = -\lambda(T)\frac{\partial T}{\partial x}, \\ \frac{\partial G}{\partial x} - \kappa_L(\rho, T)G = 0, \\ P = P(\rho, T), \quad \varepsilon = \varepsilon(\rho, T) \end{array}\right]_k, \quad (1)$$

$$k = s, l, v, g$$

$$t > 0,$$

$$x \in [\Gamma_s, \Gamma_{\mathrm{sh},s}(t)] \cup [\Gamma_{\mathrm{sh},s}(t), \Gamma_{sl}(t)] \cup [\Gamma_{sl}(t), \Gamma_{lv}(t)] \cup [\Gamma_{lv}(t), \Gamma_{vg}(t)] \cup [\Gamma_{vg}(t), \Gamma_{\mathrm{sh},g}(t)] \cup [\Gamma_{\mathrm{sh},g}(t), \Gamma_g(t)].$$

Where ρ, u, ε, T, P stand for density, gas dynamic velocity, internal energy, temperature and pressure, respectively, κ and I_ν are absorption and spectral density of plasma radiation ratios, $I_{\nu,\mathrm{eq}}$ is equilibrium radiation density, κ_L and G are absorption and density of laser radiation ratios, λ is the thermal conductivity ratio. Indices s, l, v, g denote values as belonging to solid, liquid, vapor, and gas media, respectively.

Spatial distribution of phases is provided on Fig. 1.

BOUNDARY CONDITIONS

1. For the lea-hand fixed border we set

$$x = \Gamma_s : u = 0, \quad W_T = 0, \quad W_I = 0; \quad (2)$$

2. For melting/crystallization front $x = \Gamma_{sl}$: 3 laws of conservation are formulated at the melting boundary: conservation of mass, momentum and energy captured in the reference frame moving with solid phase velocity $v_{sl} = v_{sl}^* - u_s$, where v_{sl}^* stands for velocity of the melting (crystallization) front propagation in fixed reference frame (lab):

$$\rho_s v_{sl} = \rho_l(u_l - u_s - v_{sl}),$$
$$P_s + \rho_s v_{sl}^2 = p_l + \rho_l(u_l - u_s - v_{sl})^2, \quad (3)$$
$$W_1^T - W_s^T = \rho_s v_{sl} L_m^{ne},$$

where $W_s = -\lambda(T_s)\frac{\partial T_s}{\partial x}$, $W_l = -\lambda(T_l)\frac{\partial T_l}{\partial x}$, C_{ps}, C_{pl} is thermal capacity of solid and liquid phases, respectively, $L_m^{ne} = L_m + (C_{pl} - C_{ps})(T_{sl} - T_m) + \frac{\rho_s + \rho_l}{\rho_s - \rho_l}\frac{(u_s - u_l)^2}{2}$ is non-equilibrium melting temperature.

Law of energy conservation representing a differential Stefan condition is supplemented with phenomenological condition of temperatures equality at the interphase boundary

$$T_{sl} = T_s = T_l = T_m(P_s). \quad (4)$$

The melting temperature T_m was assumed as dependent on the pressure: $T_m(P_s)$.

1. Evaporation $x = \Gamma_{1v}$: on the evaporation surface, three conservation laws are formulated in the reference frame moving with solid phase velocity, $v_{sl} = v_{sl}^* - u_s$:

$$\rho_l v_{lv} = \rho_v(u_l - u_v + v_{lv}), \quad (5)$$

$$P_l + \rho_l v_l^2 = p_v + \rho_v(u_l - u_v + v_{lv})^2, \quad (6)$$

$$W_l^T - W_v^T = -\rho_l v_{lv} L_v^{ne}, \quad W_\nu = W_\nu^l, \quad (7)$$

$$G = A(T)G_l, \quad (8)$$

where $L_v^{ne} = L_v^e(T_l) + C_{pv}(T_b - T_{lv}) + \frac{\rho_l + \rho_v}{\rho_l - \rho_v}\frac{(u_l - u_v)^2}{2}$ is non-equilibrium evaporation heat. Values T_v, ρ_v, p_v are found from the non-equilibrium Knudsen layer correspondence using the modified Crout model [28]:

$$T_v = \alpha_T(M)T_l, \quad \rho_v = \rho_H\alpha_\rho(M), \quad (9)$$

where $\alpha_T(M)$, $\alpha_\rho(M)$ are Crout coefficients, $M = \frac{u_v}{u_{\mathrm{sh}}}$ is vapor velocity in Mach numbers; ρ_H and $P_H(T_l)$ are vapor saturation pressure and density at temperature T_l.

An aluminum target ~30 μm thick situated in the air medium at a temperature $T_0 = 273$ K and under pressure $P_0 = 1$ bar was subjected to research. Values corresponding to solid and liquid aluminum phases were used as thermophysical parameters. The equilibrium melting temperature is $T_{m,0} = 933$ K. Empirical relation [29] approximated using a linear relationship $T_m(P_s) = (T_{m,0} + kP_s)$, where $k = \partial T_m/\partial P_s = 2 \times 10^{-4}$ K/bar was used as a function of $T_m(P_s)$. Critical temperature for aluminum was assumed at $T_{\mathrm{cr}} = 8 \times 10^3$ K. Starting from the temperature $T = 0.85T_{\mathrm{cr}}$, heat conductivity and laser absorption ratios were exponentially reduced in the relations, and heat capacity was exponentially increased up to critical point values of $\lambda_{\mathrm{cr}} = 0.01$ J/(K cm),

$\kappa_{crcr} = 10^3$ cm^{-1} and $C_{cr} = 10.2$ J s/(g K). Wide-range constitutive equation is used as the equation of state [30].

COMPUTING ALGORITHM

Numerical solution of the differential problem (l)–(9) was made using finite difference method with dynamic adaptation [22] allowing to do computations with direct tracking of interphase boundaries and shockwaves. As the result we can have up to 6 areas for computation with 7 boundaries, 6 of them being moving boundaries, including two shockwaves and right free boundary in the air.

RESULTS

In our simulations we used solid aluminum target is irradiated by Gaussian time profile laser pulse with duration $\tau = 10^{-15}$–10^{-8} s and peak intensity $G_0 = 10^8$–10^{16} W/cm^2. In this distribution time moment $t = 0$ corresponds to peak intensity, and calculation starts at $t = -4\tau$. For all calculations $J = G_0\tau$ changed between $1 \le J \le 50$ J/cm^2, absorption coefficient of the target $A = 10\%$. Modeling revealed that, plasma in the evaporated material is formed for J higher than 30 J/cm^2, due to the fact that plasma slows the evaporation process; the most attention was paid to the regimes prior to plasma formation.

Energy Deposition

Laser radiation energy deposits in a condensed target can be either volumetric or surface depending on laser pulse properties, thermo physical and optical properties of a target. If the length of thermal influence $l_T(a\tau)^{0.5}$ is much more than free length $l_v = \kappa^{-1}$ of energy quantum $l_T \gg l_v$ where and a is thermal diffusivity, κ is absorption coefficient, then absorption of laser radiation has the surface character, in opposite—volumetric.

According to these elementary estimates, the nanosecond mode of metals exposure is a transitory one, whereby the superficial absorption mechanism is replaced with volumetric. In pico- and femtosecond ranges, the absorption is obviously volumetric, since $l_T \ll l_v$. Thus, in the exposure modes under review, energy release in the condensed medium is volumetric. Volumetric absorption of laser radiation and the energy taken out by the flux of matter through the phase boundaries in both fractions of the target, liquid and solid, conditions are created enabling formation of near-surface temperature maximums and appearance of overheated metastable states.

General Processes

A part of the phenomena in the condensed and gas medium, are always present. The common for all the regimes is presence of phase transitions: melting and evaporation, superheated metastable states and a shockwave in gas medium. These features are typical both for all considered durations.

However as we shift from long to ultrashort pulses not only dynamics of phase transitions and metastable states changes, but also there is an occurrence of the new phenomena—shockwaves in solid phase and plasma formation in vapor or gas medium. Occurrence of the low-temperature thermal plasma 5×10^3 K $< T_{max} < 10^4$ K occurs after the end of the pulse. It is caused by forces gasdynamic squeezing, associated with propagation of the intensive shockwave generated by a powerful vapor stream.

Condensed Medium

The most important role in applications (micromashining, drilling) is played by phase transitions dynamics and their behavior depending on the pulse duration. Decreasing a laser pulse duration at the same energy density is accompanied by growth of heating velocity and, accordingly, magnification of velocity v_{sl} and, as is known [32], at $t \longrightarrow 0$ velocity of melting front $v_{sl} \sim t^{-1/2} \longrightarrow \infty$. However the actual velocity of melting front always remains limited. One of effective mechanisms of a speed v_{sl} limitation is the hydrodynamics of a molten pool [33]. Its influence can be revealed, in particular, in melting temperature dependence $T_m = T_m(P_S)$ from pressure on the melting surface P_S, which is determined by the velocity v_{sl}. As a result, growth of v_{sl} leads to growth of pressure P_S and temperatures on interphase boundary $T_{sl} = T_m(P_S)$, and the increase in melting temperature $T_m = T_m(P_S)$ restricts growth of v_{sl}.

The contribution of superheated metastable states increases with reduction of laser pulse duration τ, and in many respects define the phase transitions dynamics. A typical example of spatial structure of the solution for ultrashort $\tau = 10$ fs laser pulse at the moment of formation of shock waves in a solid phase and gas medium $t \approx 80$ fs is presented on Fig. 2.

The moment of melting front occurrence was defined by a heating of a surface of a target to equilibrium temperature of melting $T_{m,0}$. When target reached $T_{m,0}$ the liquid phase was introduced with initial thickness 0.02–0.20 nm. The volumetric mechanism of energy absorption and a mass flux through interphase boundary $x = \Gamma_{sl}$ form an undersurface temperature maximum.

At the moment, when saturated vapor pressure excides, air pressure starts the convective evaporation from the surface, the second phase transformation is introduced. Affected by quickly evaporating liquid, another undersurface temperature maximum is formed at a distance from the evaporation front, Fig. 2. The temperature maximum positions in solid and a liquid phase are defined by velocities of phase front's relation,

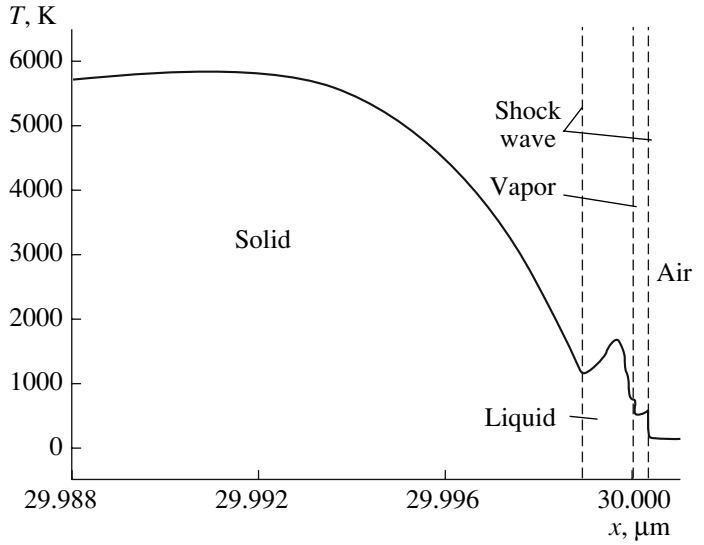

Fig. 2. Spatial temperature profile at $t = 78.5$ fs for laser pulse $\tau = 10$ fs, $G_0 = 10^{14}$ W/cm^2.

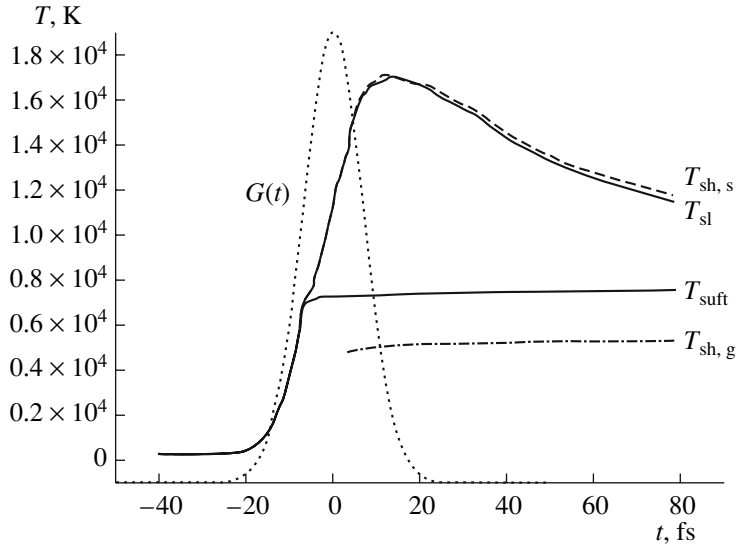

Fig. 3. Temporal profiles of temperature T_{sl}, T_{surf}, $T_{sh,\,s}$, $T_{sh,\,g}$ at the beginning and for a laser pulse $\tau = 10$ fs, $G_0 = 10^{15}$ W/cm^2.

coefficients of thermal conductivity and absorption [17]. Since the relation, $v_{sl} \gg v_{lv}$ is carried out Fig. 3 maximum of temperature in the solid phase greatly exceeds a temperature maximum in the liquid.

The main feature of sub-nanosecond interaction regimes $10^{-10} > \tau > 10^{-12}$ s close to ablation threshold $0.1 < J < 1.0$ J/cm^2 consists in that the thickness of a liquid phase does not exceed 10–20 ns and it is transparent for laser radiation. Laser pulse energy is almost completely absorbed by a solid phase, causing a considerable overheating $T_{s,\,\max} \sim 2000$ K. The absorbed energy is spent for a heating and melting of solid. Therefore melting process proceeds more effectively, and the evaporation role at low energy density $0.1 < J < 1.0$ J/cm^2 is insignificant. For ablation enhancement in picosecond range, energy density must be increased.

In ultrashort range ($10^{-15} < \tau \le 10^{-12}$ s) at $1 \le J \le 10$ J/cm^2 fast heating of a target, high melting front velocity and rather slow energy transmission by thermal conduction lead to significantly higher level of solid state in comparison with longer pulses. The peak velocity of melting front at $\tau \approx 10^{-13}$–10^{-15} s reaches sonic velocity which for Al ~ 6.26×10^3 m/s. As v_{sl} approaches sonic velocity, it premises on the one hand

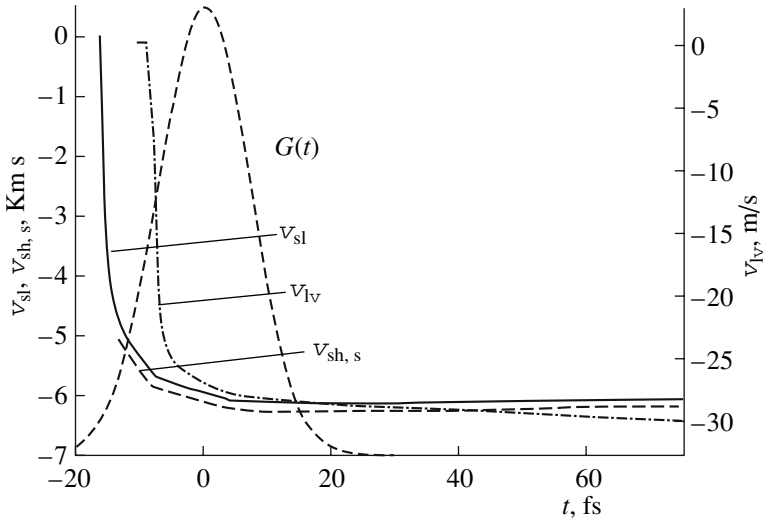

Fig. 4. Temporal profiles of melting front velocity v_{sl}, shockwave velocity $v_{sh,\,g}$, evaporation front velocity v_{lv}, for a laser pulse $\tau = 10$ fs, $G_0 = 10^{15}$ W/cm^2.

for shockwave formation in solid phase, and with another—facilitates its overheating Fig. 2. For a laser pulse $\tau = 10$ fs. $J = 1$ J/cm^2, at the moment of shockwaves formation $t \approx 80$ fs in surrounding gas and in solid phase, the temperature maximum is about 6000 K and is situated on depth ~20 nm from the boundary $\Gamma_{sl}(t)$. The overheating degree $T_{s,\,\max}/T_{m0}$ reaches about 6.5. Correspondingly velocity, temperature and pressure on the interphase boundary $\Gamma_{sl}(t)$ are $v_{sl} = 4 \times 10^3$ m/s, $T_{sl} \gg T_{m0} \approx 1.5 \times 10^3$ K, and $P_s \approx 0.5$ Mbar. This pressure appears enough for formation of the strong shockwave in the solid phase.

With increase of energy density $J = 10$ J/cm^2 at the same pulse duration leads to sharp increasement of all overheating parametres, Fig. 3. On Figs. 3 and 4 temporary profile of temperature on interphase boundaries $T_{\rm surf}(t)$, $T_{sl}(t)$ front of shock waves $T_{sh,\,s}(t)$, $T_{sh,\,g}(t)$, and also corresponding velocities are presented $v_{sl}(t)$, $v_{lv}(t)$, $v_{sh}(t)$. From curves it follows, that phase transitions and a shockwave in the solid phase arise on the leading edge of a laser pulse. On the falling edge, there is a shockwave in gas medium. In the middle of a pulse velocity of melting front reaches it's maximum velocity, sonic velocity $v_{sl} = 6.26 \times 10^3$ m/s, making overheat degree $T_{s,\,\max}/T_{m0} \approx 20$. The melting front and shockwave front have nearly identical velocities and temperatures and are spreading as a complex. The energy accumulated in a solid phase has stabilizing influence on temperature of an evaporated surface, which reaches $T_{\rm surf} \approx 7 \times 10^3$ K, and remains constant until the complete vanishing of the overheating. Velocities of shockwaves and phase fronts also remain constant, Fig. 4. To the moment $t \approx 2.5 \times 10^{-8}$ s redundant energy is completely carried out from the overheated area and spatial distribution of temperature any more does not contain near surface maximums, Fig. 5. So long-lived, in comparison with duration of a laser pulse, energy redistribution is defined by prevalence of relatively slow conductive mechanism of heat transfer. Slow redistribution of energy leads to increase in molten pool and evaporated material thickness. Thus the melting front in $t \approx 0.5 \times 10^{-8}$ s after the end of a pulse moves with sonic velocity together with the shockwave front. With reduction of temperature gradients in the area of phase boundary, the velocity v_{sl} falls, and the uniform complex from melting front and a shockwave breaks up. The shock wave becomes decaying, its leading edge with sonic velocity leaves far forward, Fig. 5.

The surface evaporation up to $t \approx 0.8 \times 10^{-8}$ s occurs with the greatest possible velocity, number of Mach on exterior boundary of Knudsen layer, M = 1, Fig. 6. By this moment $t \approx 0.8 \times 10^{-8}$ s in gas medium there is plasma formation by means of the gas-dynamical squeezings, pressure in these plasma areas exceeds pressure of saturated vapor and that is slowdowning down the flux of the evaporated material. The number of Mach continuously decreases and to the time $t \approx 2.5 \times 10^{-8}$ s is equal to zero, M = 0, Fig. 6, that formally corresponds to the termination of the evaporation process. The evaporation ends, in spite of the fact that the surface temperature for this moment is $T_{\rm surf} \approx 3700$ K exceeds the boiling temperature for aluminum $T_b \approx 2730$ K.

In picosecond range we can see the same pattern of processes. Figure 7 shows the spatial distribution of temperature at the moment $t \approx 2.5 \times 10^{-8}$ s testifies. During pulse action the small amount of liquid appears. Liquid phase thickness does not exceed the value of 30 nm during pulse action. Due to the clearance of liquid around critical point it is almost transparent for

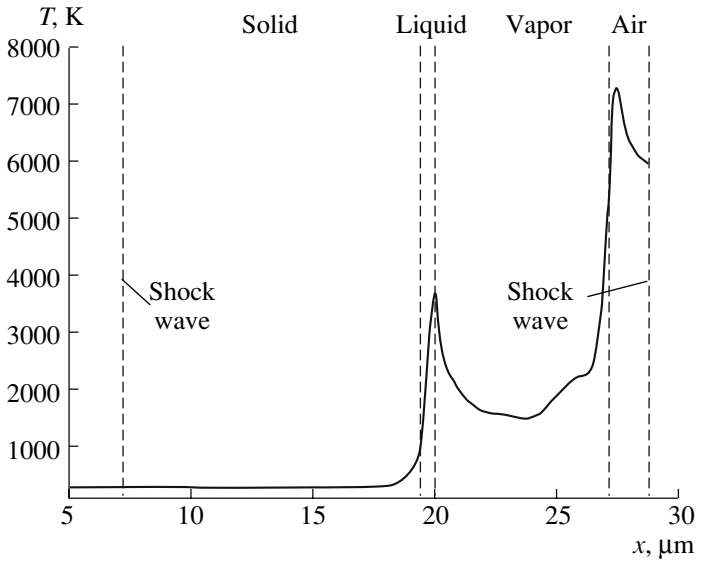

Fig. 5. Spatial profile of temperature at $t = 2.5$ ns for a laser pulse $\tau = 10$ fs, $G_0 = 10^{15}$ W/cm^2.

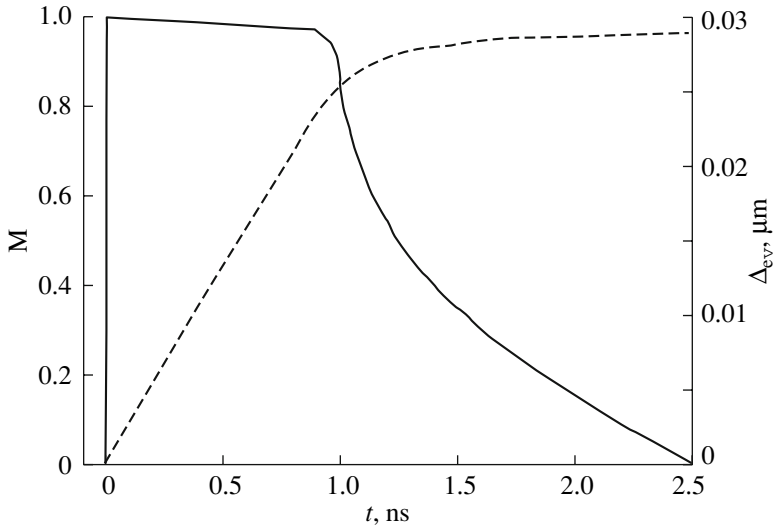

Fig. 6. Temporal profiles of the evaporation velocity in Mach numbers at outer Knudsen layer for a laser pulse $\tau = 10$ fs, $G_0 = 10^{15}$ W/cm^2.

laser irradiation. As the result we have almost constant temperature $T_{sl} = T_{lv}$ in liquid. After the end of the pulse action the saved energy of the overheated solid phase is spent on heating of liquid phase and maintaining high temperature on the surface. This provides much longer evaporation time, than pulse duration.

Since energy transfer from overheated solid to liquid phase is implemented by relatively slow mechanism of thermo conductivity, evaporation time is almost the same for pico- and femtosecond laser pulse and is about 2.5–3.0 ns, Fig. 8. Near surface temperature maximums completely disappear at the moment $t = 2.0$–2.2 ns, Figs. 3 and 7.

Dynamics of the phase transitions undergoes essential changes with shifting laser pulses duration. On Figs. 9 and 10 there are dependences of the peak values of velocities of melting v_{sl}, evaporation v_{lv}, a molten pool Δ_l, and the evaporated layer Δ_{ev} vs. duration of laser pulses Their analysis has shown, that at long pulses $10^{-8} \geq \tau \geq 10^{-9}$ s and densities of energy $1 \leq J \leq 10$ J/cm^2 melting and evaporation take place under usual scheme. The temperature of the surface $T_{sur} \approx (5.7–7.2) \times 10^3$ K and velocity of the evaporation front

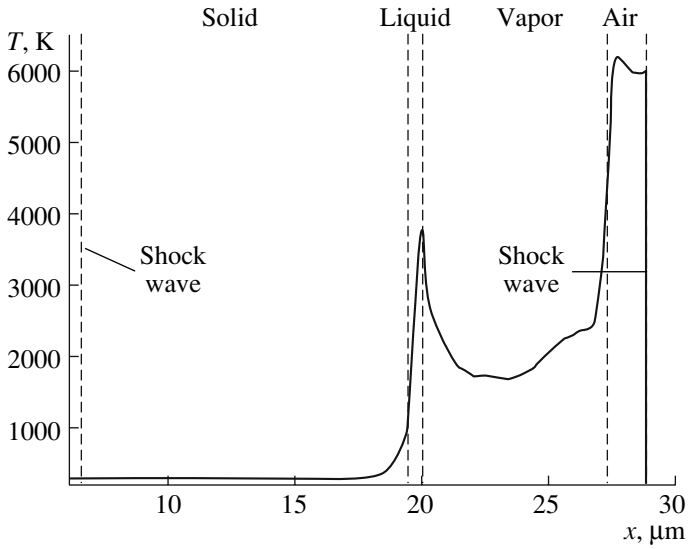

Fig. 7. Spatial profile of temperature at $t = 2.5$ ns for a laser pulse $\tau = 1.0$ ps, $G_0 = 10^3$ W/cm^2.

$v_{lv} \approx 10$–27 m/s with small delay follow changes of radiation intensity. The peak melting front velocity is between 50–500 m/s, Fig. 9. The maximum thickness of a molten pool increases with duration and reaches a maximum at $\tau = 10^{-8}$ s ($\Delta_l \approx 1.9$ μm), Fig. 10. Evaporated layer Δ_{ev} is more than one order of magnitude less.

Pressure on a surface of solid phase P_s does not exceed 4×10^8 Pa. The temperature T_{sl} on interphase boundary at such pressure practically does not differ from equilibrium $T_{sl} \cong T_{m0}$. The undersurface temperature maximum is situated on some distance from the boundary Γ_{sl} and its value exceeds value of equilibrium melting temperature on a few tens degrees. Its presence increases lifetime of a molten pool and duration of the evaporation process which at $\tau \cong 10^{-8}$ s appears in 2.5 times longer than pulse duration, Fig. 8.

Time dependence of maximum molten pool thickness $\Delta_l(\tau)$, maximum evaporated layer $\Delta_{ev}(\tau)$ curves are falling with decreasing of τ and vary in a range, $\Delta_l(\tau) \sim$ (1.95–0.60) μm, and $\Delta_{ev}(\tau) \sim$ (0.130–0.023) μm, Fig. 4. We underline, that the thickness of the evaporated material is in good correspondance with experimental data [15]. Thus, thanks to occurrence of superheated metastable states reduction of laser pulses duration by 4–7 orders leads to reduction of thickness, $\Delta_l(\tau)$, $\Delta_{ev}(\tau)$ only in 3–6 times. Becouse of $v_{sl} \gg v_{lv}$, Fig. 9, depth of the molten pool $\Delta_l(\tau)$ in all investigated time range appears much more than the evaporated layer thickness, $\Delta_{ev}(\tau)$ and their ratio is $\Delta_l(\tau)/\Delta_{ev}(\tau) = 10$–30, Fig. 10. However, in a femtosecond range, where the temperature of metastable states comes nearer or exceeds critical temperature, it is necessary to expect change of the surfacemechanism of evaporation by the volumetric one with a high probability.

Gas Medium

The condition of vapor near to boundary with a liquid in prior plasma mode is mainly defined by temperature on a vaporizing surface and a thermal conduction of a liquid. Thus, a heating vapor by absorption of laser irradiation for which it is practically transparent is negligible.

In gas medium promptly expanding vapor flux, with gasdynamical velocity near to contact boundary reach-

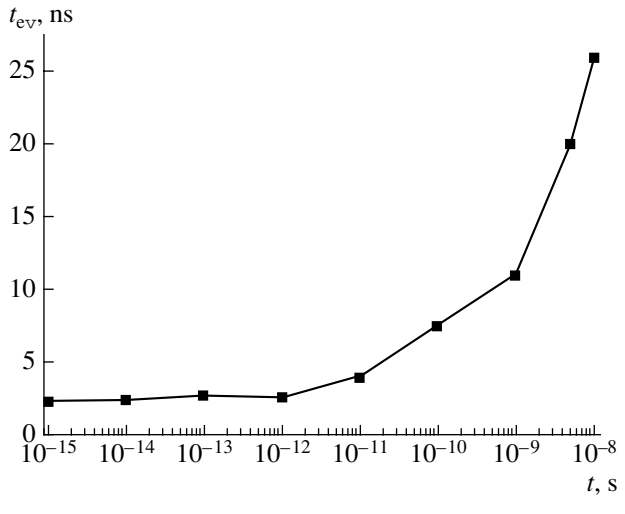

Fig. 8. Dependences of evaporation duration on duration of the laser pulse.

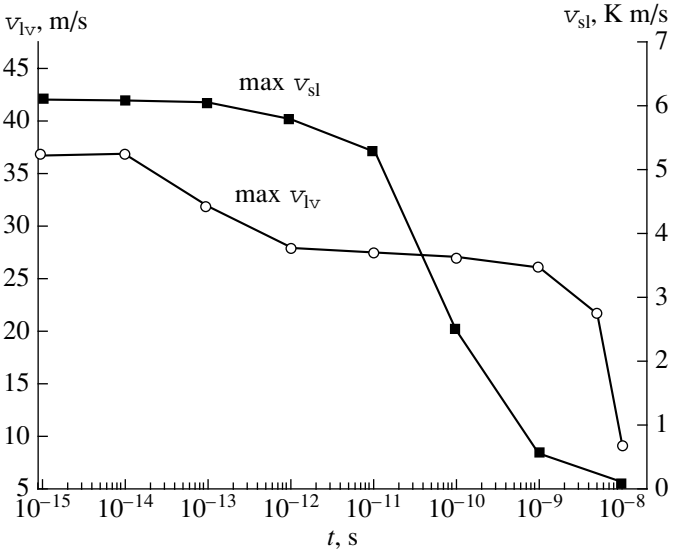

Fig. 9. Dependences of maximum velocities of the melting front $v_{sl}(\tau)$ and the evaporation front $v_{lv}(\tau)$ on laser pulse duration τ.

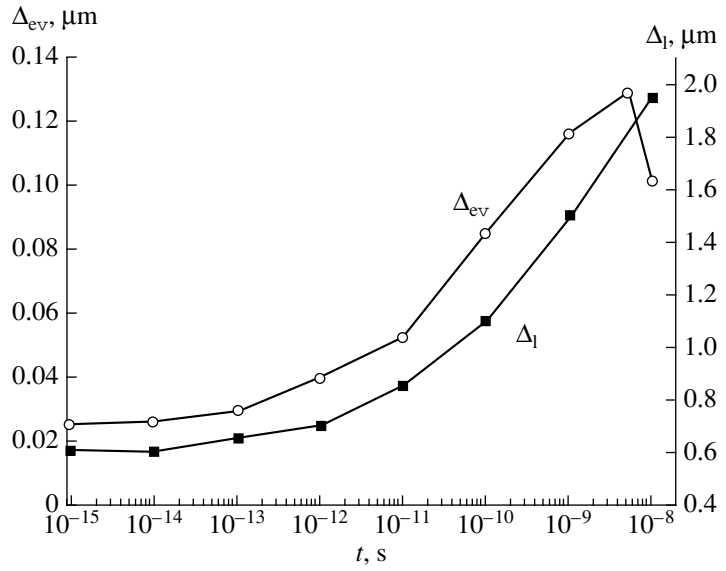

Fig. 10. Dependences of the molten pool $\Delta_l(\tau)$ the evaporated layer thicknesses $\Delta_{ev}(\tau)$ from laser pulse duration τ.

ing several kilometers per second, works as the accelerated piston, which is pushing out cold air. Starting from a certain instant, it leads to shockwave formation in gas. Explicitly determined by means Rankine–Hugoniot conditions the shockwave is spread towards the laser radiation. Considerably later after the termination of laser pulse forces of squeezing in gas medium create the low-temperature thermal plasma.

The typical example of spatial structure of the solution gained for ultrashort (τ = 10 fs) influence at the moment of intense plasma formation $t \approx 2.5$ ns is presented on Fig. 2. The peak temperature of plasma reaches $T_{max} \approx 7400$ K and is behind front of a shockwave near to contact boundary of vapor–air. The spatial size of vapor area during laser pulse influence is insignificant ~7 nm, but to the end of evaporation reaches 7500 nm, Fig. 5.

If the intensity is high enough $G > 10^{16}$ W/cm^2, avalanche growth of temperature, concentration of charged particles and absorption coefficient near evaporation surface begins. This process of high ionized and absorbing plasma formation is equilibrium analog of optical breakthrough. Vapor temperature rises up to 10^6 K fast, electron concentration $N_e = 8 \times 10^{22}$ cm^{-3}, absorption coefficient $\kappa \approx 10^5$ cm^{-1}. A shockwave appears which expands in direction from the surface reaches the first shockwave in gas and absorbs it. Decrease of laser irradiation on the surface of the target caused by growth of pressure in plasma leads to elimination of surface evaporation.

CONCLUSIONS

Our analysis shows that long and ultrashort pulses at the same energy density J are essentially different with mechanisms of laser energy transformation.

For long impulses $\tau \sim 10$ ns, there is small overheating of a solid phase (tens degrees) which amplifiers in 2.5 times time of evaporation from laser pulse duration. The most of laser pulse energy is spent for melting and evaporation processes. The rest—is spent for heating of a solid phase and shockwave generation in gas medium.

With shifting to ultrashort laser pulse duration the increasing part of laser pulse energy is spent for metastable states superheating in a condensed medium and generation of shock waves in a solid phase and gas medium. The smaller share of energy is spent for evaporation process. So, if at 10 ns pulse duration the relation of thickness $\Delta_l(\tau)/\Delta_{ev}(\tau)$ did not exceed 20 at 1 fs pulse duration it reaches 30.

In femtosecond range, the quantity the solid phase overheating reaches values T_{max}/T_{m0} = 8–10, and near surface temperature maximum becomes close to critical temperature. In these situations there is a great probability of spinodal decay of metastable states or a nucleation of a new phase that corresponds to the shift from surface mechanisms of phase transformations to volumetric ones.

ACKNOWLEDGMENTS

This study was partly supported by Russian Foundation for Basic Research grants nos. 07-07-00045-a, RFBR-DFG-08-07-91950.

REFERENCES

1. W. W. Duley, *UV Lasers: Effects and Applications in Materials Science* (Cambridge Univ., Cambridge, 1996).
2. V. L. Mazhukin and A. A. Samarskii, Math. Surv. Math. Industry **4**, 85 (1994).
3. K. Sokolowski-Tinten and D. von der Linde, Phys. Rev. B **61**, 2643 (2000).
4. V. M. Gordienko, M. S. Dzhidzhoev, V. V. Kolchin, et al., Kvant. Electron. **25**, 158 (1995) [Quantum Electron. **25**, 146 (1995)].
5. *Laser Ablation. Principles and Applications*, Ed. by J. C. Miller (Springer, Berlin, 1994).
6. A. A. Vedenov and G. G. Gladush, *Physical Processes at Laser Handling of Materials* (Energoatomizdat, Moscow, 1985).
7. *Proc. of the Institute of General Physics Academy of Sciences of the USSR*, Ed. by A. M. Prokhorov (Nova Science Publ., New York, 1990), vol. 13.
8. V. I. Mazhukin, M. G. Lobok, and I. Smurov, Appl. Surf. Sci. **253**, 7744 (2007).
9. G. P. Pinho, H. Schittenhelm, W. W. Duley, S. A. Schueter, H. R. Jamani, and R. E. Mueller, Appl. Surf. Sci. **127–129**, 983 (1998).
10. V. I. Mazhukin, V. V. Nossov, and I. Smurov, J. Appl. Phys. **101**, 24922 (2007).
11. A. Peterlongo, A. Miotello, and R. Kelly, Phys. Rev. E **50**, 4716 (1994).
12. D. von der Linde, Science **302**, 1345 (2003).
13. H. Iglev, M. Schmeisser, K. Simeonidis, A. Thaller, and A. Laubereau, Nature **439**, 183 (2006).
14. B. N. Chichkov, C. Momma, S. Nolte, F. von Alvensleben, and A. Tunnermann, Appl. Phys. A: Solids Surf. **63**, 109 (1996).
15. M. D. Shirk and P. A. Molian, J. Laser Appl. **10**, 18 (1998).
16. K. Sokolowski-Tinten and D. von der Linde, J. Phys. Cond. Mat. **16**, R1517 (2004).
17. D. Boschetto, E. G. Gamaly, A. V. Rode, B. Luther-Davies, D. Glijer, T. Garl, O. Albert, A. Rousse, and J. Etchepare, Phys. Rev. Lett. **100**, 027404 (2008).
18. E. G. Gamaly, A. V. Rode, V. T. Tikhonchuk, et al., Phys. Plasmas **9**, 949 (2002).
19. Zh. Lin and L. V. Zhigilei, Proc. SPIE **6261**, 62610U-1 (2006).
20. G. I. Alferov, Yu. V. Kovalchuk, Yu. V. Pogorelsky, and O. V. Smolsky, Izv. AN SSSR, Ser. Fiz. **49**, 1069 (1985).
21. X. Xu, C.Grigoropoulos, and R. E. Russo, Appl. Phys. Lett. **65**, 1745 (1994).
22. V. I. Mazhukin, I. Smurov, G. Flamant, and C. Dupuy, J. Thin Solid Films **241**, 109 (1994).
23. V. L. Mazhukin, I. Smurov, and G. Flamant, J. Appl. Phys. **78**, 1259 (1995).
24. S.Williamson, C. Mourou, and J. C. H. Li. Phys. Rev. Lett. **52**, 2364 (1984).
25. M. Kandyla, T. Shih, and E. Mazur, Phys. Rev. B **75**, 214107 (2007).
26. D. Ivanov and L. V. Zhigilei, Phys. Rev. B **68**, 064114-1 (2003).
27. D. Ivanov and L. V. Zhigilei, Phys. Rev. Lett. **98**, 195701-1 (2007).
28. V. I. Mazhukin, P. A. Prudkovskii, and A. A. Samokhin, Matem. Modelirov. **5**, 3 (1993).
29. J. Lees and B. H. J. Williamson, Nature Phys. **208**, T84 (1965).
30. K. S. HoIian, J. Appl. Phys. **59**, 149 (1986).
31. P. V. Breslavsky and V. I. Mazhukin, Comput. Math. Math. Phys. **47**, 687 (2007).
32. H. S. Carslaw and J. C. Jaeger, *Conduction of Heat in Solids* (Clarendon, Oxford, 1959).
33. P. V. Breslavsky, V. I. Mazhukin, and A. A. Samokhin, Dokl. Akad. Nauk SSSR **320**, 1088 (1991) [Sov. Phys. Dokl. **36**, 682 (1991)].